PHILOSOPHICAL TRANSACTIONS OF THE ROYAL SOCIETY A MATHEMATICAL, PHYSICAL & ENGINEERING SCIENCES

Boundary–layer flow along a ridge: alternatives to the Falkner–Skan solutions

Peter W. Duck, Simon R. Stow and Manhar R. Dhanak

Phil. Trans. R. Soc. Lond. A 2000 **358**, 3075-3090
doi: 10.1098/rsta.2000.0697

10.1098/rsta.2000.0697

THE ROYAL SOCIETY

Boundary-layer flow along a ridge: alternatives to the Falkner–Skan solutions

By Peter W. Duck[1], Simon R. Stow[1]† and Manhar R. Dhanak[2]

[1]*Department of Mathematics, University of Manchester, Oxford Road, Manchester M13 9PL, UK*
[2]*Department of Ocean Engineering, Florida Atlantic University, Boca Raton, FL 33431, USA*

We consider the laminar boundary-layer flow past a semi-infinite plate with a streamwise ridge. We seek similarity solutions to the problem, when the freestream velocity takes the form x^{*n}, where x^* denotes the distance from the leading edge of the plate; such solutions may exist if the transverse and lateral scales of the ridge develop in the streamwise direction at the same rate as the boundary-layer thickness grows. In deriving the necessary far-field boundary conditions for these calculations, we are led to a consideration of a class of flows of the Falkner–Skan type, but which may possess a cross-flow component of velocity (which grows linearly in the cross-flow direction). This new class of flow is a three-dimensional alternative to the Falkner–Skan family. Wall transpiration effects are also addressed and portions of the solution curves correspond to separated flows. Solutions for the flow along a ridge for both the aforementioned classes of far-field behaviour are presented.

A study of the effects of relaxing the similarity constraint on both the classical solution and new families of solution is also made. It is found that the problem is (frequently) complicated by the existence of spatially developing eigensolutions (originating from the leading edge), which have the effect of rendering standard parabolic marching procedures ill posed.

Keywords: three-dimensional boundary layers; flows along a ridge; Falkner–Skan; non-uniqueness; similarity solutions

1. Introduction

The Falkner–Skan family of solutions (see, for example, Rosenhead 1966) represents one of the key building blocks of classical boundary-layer theory. Freestream velocities which vary algebraically in the streamwise direction encompass a broad spectrum of both theoretically and practically important configurations. It is well known that for freestream velocity variations of the form x^{*n} (x^* representing the streamwise coordinate, origin at some leading edge), non-uniqueness of two-dimensional, similarity-type, boundary-layer solutions occurs for $n < 0$, with two solutions in the range $n_0 < n < 0$, where $n_0 \approx -0.0904$ (as determined by Hartree (1937)), there being no (connecting) solutions for $n < n_0$. One of the two solutions corresponds to entirely forward flow, the other to partly reversed flow. In the limit $n \to 0-$, the

† Present address: Department of Engineering, University of Cambridge, Cambridge CB2 1PZ, UK.

latter solution corresponds to a massively displaced shear layer, lying above a region of relatively stagnant flow (see Stewartson (1954) and also Duck *et al*. (1999), which is hereafter referred to as DSD).

In a recent study, Dhanak & Duck (1997) (hereafter referred to as DD) found that non-uniqueness in similarity solutions to three-dimensional corner boundary-layer flows was quite common. In particular, DD found that for freestream velocity variations of the form x^{*n} with imposed symmetry about the line bisecting the corner angle, *at least* two similarity-type solutions exist for $n > -0.018$ (approximately). In fact, for $n < 0$ and $|n| \ll 1$, four solutions were found; these observations confirmed and extended those of Ridha (1992). In the case of flows not possessing the aforementioned symmetry condition, the overall picture can be even more complicated, with the possibility of additional solutions.

One of the key observations of DD is that in the case of zero streamwise pressure gradient flows over a flat plate (i.e. $n = 0$ in the above notation), in addition to the classical Blasius solution, a second, three-dimensional solution is also possible in which the cross-flow velocity takes the form of a jet-like motion, accelerating linearly in the cross-flow direction. Although this conclusion was found in the context of corner boundary layers (with the imposed symmetry condition), in the special case of $n = 0$ these conclusions are also applicable to the class of flows with zero cross-flow at the outer edge of the boundary layer; this may be partly regarded as a corollary. It is this observation that provides the impetus for this paper, namely to study three-dimensional boundary-layer flows over non-flat surfaces. Flows of this new type may be regarded as a useful and important extension (and in many cases an alternative) to the Falkner–Skan–Cooke family of solutions (the latter class having no cross-flow variation). As such, flows of the type considered here are likely to be useful in the context of wing–body junctions, for example.

To illustrate the applicability of these (similarity) solutions, we consider the laminar boundary-layer flow over a streamwise surface ridge, the transverse and lateral dimensions of the ridge being comparable with the boundary-layer thickness; the similarity constraint is retained in this respect. This problem is formulated in § 2. In § 3 we consider the nature of the solution at large distances from the ridge, which, just as in DD, is important both in determining accurate far-field boundary conditions and in understanding the nature of the various solution branches. In § 4 we present numerical solutions to the problem as formulated in § 2. In § 5 we discuss our conclusions and raise some further issues, in particular the nature of the flow with the similarity constraint relaxed (i.e. streamwise developing flows). In DSD it was found that the corresponding solutions related to corner-flow problems were frequently greatly complicated by the existence of spatial eigenvalues, originating from the leading edge (i.e. $x^* = 0$). These render standard parabolic marching schemes inappropriate (in particular these are ill posed under these circumstances). In the present study we find that the occurrence of such leading-edge eigensolutions is also quite common. We give details of circumstances when these exist.

2. Formulation

The schematic of the problem to be considered is shown in figure 1. We take a system of Cartesian coordinates (Lx, Ly, Lz), where L is a reference length-scale (generally the spatial scale of the freestream velocity variation). For $x > 0$ we assume that

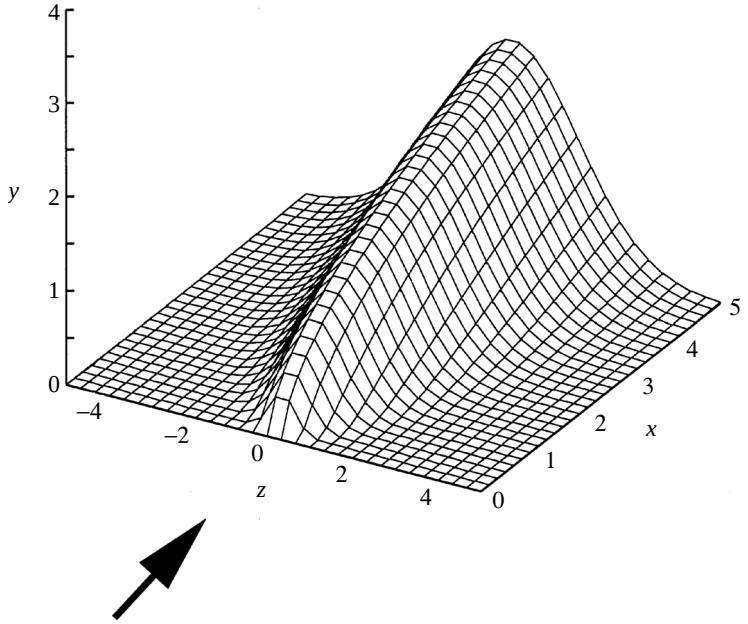

Figure 1. Schematic of the problem.

some (non-planar) surface lies in the path of the freestream flow (the leading edge of the surface is taken to be straight, and lies along $x = 0$). If the plate distortions are finite in the longitudinal extent (the situation we shall be focusing on in this paper), then it is convenient to choose the flat, undistorted surface to coincide with the plane $y = 0$, and with the cross-flow direction corresponding to the z-direction. The velocity is written as $U_\infty(u, v, w)$, such that at the outer edge of the boundary layer (that develops on the plate) the velocity in the streamwise (x) direction is written $U_\infty F(x)$. We define the Reynolds number $Re = (U_\infty L)/\nu$, and *assume* that the ridge is of height $O(LRe^{-1/2})$ and the cross-flow scale is of the same order, leading to transverse and cross-flow velocities of $O(U_\infty Re^{-1/2})$; ν represents the kinematic viscosity (assumed to be constant).

We expect that the boundary layer developing from the leading edge ($x = 0$) takes on the following asymptotic form as $Re \to \infty$ (guided by the corner-flow works of Rubin (1966) and by DD and DSD):

$$\left.\begin{aligned} u &= \hat{U}(x, Y, Z) + \cdots, \\ p &= P_0(x) + Re^{-1/2} P_1(x) + Re^{-1} \hat{P}(x, Y, Z) + \cdots, \\ v &= Re^{-1/2} \hat{V}(x, Y, Z) + \cdots, \\ w &= Re^{-1/2} \hat{W}(x, Y, Z) + \cdots, \end{aligned}\right\} \tag{2.1}$$

where $\rho U_\infty^2 p$ denotes the pressure, and ρ is the density (assumed to be constant so that the fluid is regarded as incompressible). In (2.1) we have also introduced scaled transverse and cross-flow coordinates, namely $Y = Re^{1/2} y$, $Z = Re^{1/2} z$, and P_0 and P_1 can be shown to be independent of Y and Z.

Substitution of (2.1) into the Navier–Stokes and continuity equations, and taking the leading-order terms gives

$$\hat{U}\hat{U}_x + \hat{V}\hat{U}_Y + \hat{W}\hat{U}_Z = \hat{U}_{YY} + \hat{U}_{ZZ} - P_{0_x}, \tag{2.2}$$

$$\hat{U}\hat{V}_x + \hat{V}\hat{V}_Y + \hat{W}\hat{V}_Z = \hat{V}_{YY} + \hat{V}_{ZZ} - \hat{P}_Y, \tag{2.3}$$

$$\hat{U}\hat{W}_x + \hat{V}\hat{W}_Y + \hat{W}\hat{W}_Z = \hat{W}_{YY} + \hat{W}_{ZZ} - \hat{P}_Z, \tag{2.4}$$

$$\hat{U}_x + \hat{V}_Y + \hat{W}_Z = 0. \tag{2.5}$$

The boundary conditions are that $\hat{U} = \hat{W} = 0$, $\hat{V} = \hat{V}_{\mathrm{w}}(x, Z)$ on the wall (which is taken to lie along $Y = H^*(x, Z)$, the ridge profile), and $\hat{U} \to F(x)$, $\hat{W} \to 0$ as $Y \to \infty$; the V_{w} term admits the inclusion of transpiration through the surface.

The condition on $\hat{U}$ as $Y \to \infty$ leads to the condition that the leading-order pressure gradient is given by $P_{0x} = -FF_x$, while the $O(Re^{-1})$ pressure term, although of relatively small order, is vital here to leading order, just as in Rubin (1966), DD and DSD.

For most of this paper we focus our attention on similarity-type solutions corresponding to $F(x) = x^n$, (following DD). To be consistent with this, we write

$$\hat{U} = x^n U(\eta, \zeta), \tag{2.6}$$

$$\hat{V} = x^{(n-1)/2} V(\eta, \zeta) = \frac{x^{(n-1)/2}}{\sqrt{2}}[(1-n)(\eta + H(\zeta))U - \Phi], \tag{2.7}$$

$$\hat{W} = x^{(n-1)/2} W(\eta, \zeta) = \frac{x^{(n-1)/2}}{\sqrt{2}}[(1-n)\zeta U - \Psi], \tag{2.8}$$

$$P_0 = -\tfrac{1}{2}x^{2n}, \qquad \hat{P} = x^{n-1}P(\eta, \zeta), \tag{2.9}$$

where

$$\eta = Y/\sqrt{2}\xi - H(\zeta), \qquad \zeta = Z/\sqrt{2}\xi, \qquad \xi = x^{(1-n)/2}, \tag{2.10}$$

and where $H^*(x, Z) = x^{(n-1)/2}H(\zeta)$ and $\hat{V}_{\mathrm{w}}(x, Z) = x^{(n-1)/2}V_{\mathrm{w}}(\zeta)$, for consistency with the similarity form. The $\Phi(\eta, \zeta)$ and $\Psi(\eta, \zeta)$ serve as vector potentials, and (η, ζ) form a system of body-fitted coordinates, such that the plate surface lies along $\eta = 0$. The boundary-layer equations (2.2)–(2.5) may then be manipulated into the following form:

$$2U = \Phi_\eta + \Psi_\zeta - H'\Psi_\eta, \tag{2.11}$$

$$(1 + H'^2)U_{\eta\eta} + U_{\zeta\zeta} - 2H'U_{\eta\zeta} - H''U_\eta + 2n = 2nU^2 - \Phi U_\eta - \Psi(U_\zeta - H'U_\eta), \tag{2.12}$$

$$(1 + H'^2)\theta_{\eta\eta} + \theta_{\zeta\zeta} - 2H'\theta_{\eta\zeta} + 2(1-n^2)[(\eta + H)U(U_\zeta - H'U_\eta) - \zeta U U_\eta] + \Phi\theta_\eta + \Psi(\theta_\zeta - H'\theta_\eta) + 2U\theta - H''\theta_\eta = 0, \tag{2.13}$$

where in the above we have introduced a streamwise vorticity function, namely

$$\theta = \Psi_\eta - \Phi_\zeta + H'\Phi_\eta. \tag{2.14}$$

The boundary conditions to be applied to this system are

$$U = \Psi = 0, \quad \Phi = \Phi_{\mathrm{w}} \quad \text{on } \eta = 0, \tag{2.15}$$

$$U \to 1, \quad \Psi \to \zeta(1-n) \quad \text{as } \eta \to \infty, \tag{2.16}$$

where $\Phi_{\rm w} = -\sqrt{2}V_{\rm w}^*$. Note that the condition (2.16) arises from the condition that there is no cross-flow velocity component in the freestream.

In the following section we consider limiting forms of the system (2.11)–(2.14) valid at large distances from the distortion, assuming surface distortions of finite extent in the cross-flow (ζ) direction.

3. Solutions for $|\zeta| \to \infty$

In the work on corner boundary layers of DD and DSD it was found that the nature of the solution at large distances from the corner was absolutely crucial in

(i) determining accurate far-field (boundary) conditions to the full problem, and

(ii) understanding the nature of various solution branches.

In the present study, this is equally true. To this end, following these previous studies, we expect that as $|\zeta| \to \infty$:

$$\left.\begin{aligned} U(\eta,\zeta) &= U_0(\eta) + \zeta^{-1}U_1(\eta) + O(\zeta^{-2}),\\ \Phi(\eta,\zeta) &= \Phi_0(\eta) + \zeta^{-1}\Phi_1(\eta) + O(\zeta^{-2}),\\ \Psi(\eta,\zeta) &= \zeta\Psi_0(\eta) + \Psi_1(\eta) + O(\zeta^{-1}),\\ \theta(\eta,\zeta) &= \zeta\theta_0(\eta) + \theta_1(\eta) + O(\zeta^{-1}),\\ W(\eta,\zeta) &= \zeta W_0(\eta) + W_1(\eta) + O(\zeta^{-1}). \end{aligned}\right\} \tag{3.1}$$

Taking the leading-order terms from (2.11)–(2.14) in this limit leads to the following set of equations

$$2U_0 = \Phi_{0\eta} + \Psi_0, \tag{3.2}$$

$$U_{0\eta\eta} + 2n = 2nU_0^2 - \Phi_0 U_{0\eta}, \tag{3.3}$$

$$\theta_0 = \Psi_{0\eta}, \tag{3.4}$$

$$\theta_{0\eta\eta} - 2(1-n^2)U_0U_{0\eta} + \theta_{0\eta}\Phi_0 + \Psi_0\theta_0 + 2U_0\theta_0 = 0. \tag{3.5}$$

The boundary conditions to be applied are

$$U_0(0) = \Psi_0(0) = 0, \qquad \Phi_0(0) = g(0) = \Phi_{0\rm w} = \Phi_{\rm w}(\zeta \to \infty), \tag{3.6}$$

$$U_0 \to 1, \quad \theta_0 \to 0, \quad \Psi_0 \to \Psi_{0\rm e} \quad \text{as } \eta \to \infty. \tag{3.7}$$

The term $g(0)$ has been introduced here as a measure of the transpiration. We have assumed implicitly that as $|\zeta| \to \infty$:

(i) $H(\zeta) = o(\zeta^{-2})$ (although other, slower rates of function decay, and even certain classes of growth, could, in principle, be accommodated into the model);

(ii) the transpiration parameter $\Phi_{\rm w} \to g(0) = O(1)$; and

(iii) $\Psi \to \zeta\Psi_{0\rm e}$, $\Psi_{0\rm e} = O(1)$ as $\zeta \to \infty$.

Crucially, it is important to note that although the above has been derived in the context of the far-field development of the flow past a ridge, its applicability is considerably broader. In particular, the leading-order system developed above is also

relevant to a three-dimensional extension to the Falkner–Skan family of solutions of the form (where $\eta = Y/\sqrt{2}\xi$)

$$u = x^n U_0(\eta), \qquad v = Re^{-1/2} x^{(n-1)/2} V_0(\eta), \qquad w = z x^{n-1} W_0(\eta). \tag{3.8}$$

The key point is that the cross-flow velocity component is allowed to grow linearly in the cross-flow direction; the other two velocity components are independent of the cross-flow coordinate.

The above system is identical to eqns (3.5)–(3.10) of DD, except for the inclusion of transpiration effects (i.e. $g(0)$). Further, in DD, although most of the attention was focused on corner flows with symmetry (corresponding to $\Psi_{0e} = 1$), some results were presented in this limiting case for asymmetric flows with specified secondary flow direction along the corner-bisector line (a parameter λ was introduced).† Here, an alternative class of flows will be sought for which $W(\eta \to \infty) \to 0$, which corresponds to zero cross-flow velocity external to the boundary layer (at least to leading order), which, in the present context, leads to the condition that $\Psi_{0e} = 1 - n$, or, in the notation of DD, $\lambda = n + 1$.

It was noted in DD that one solution of the above system is

$$\left.\begin{aligned} U_0 &= F_0'(\eta), & \Phi_0 &= (n+1)F_0(\eta), \\ \Psi_0 &= (1-n)F_0'(\eta), & \theta_0 &= (1-n)F_0''(\eta), \end{aligned}\right\} \tag{3.9}$$

where

$$F_0''' + 2n = 2nF_0'^2 - (n+1)F_0F_0'', \tag{3.10}$$

which is the Falkner–Skan equation (Rosenhead 1966). In the context of DD, this particular solution was only useful when $n = 0$, i.e. the zero-pressure-gradient case corresponding to the Blasius equation, on account of the symmetry constraint; in the present context, this is a perfectly useful far-field solution, yielding zero cross-flow velocity outside of the boundary layer as required (zero cross-flow velocity across the entire boundary layer in fact). However, in DD, for $n = 0$ a second solution was also found, comprising a cross-flow jet-like motion. A corollary of this is that such solutions, also involving a non-zero jet-flow motion, are likely to occur for other values of n. The system (3.2)–(3.7) was, therefore, computed, using both Runge–Kutta and finite-difference techniques.

We now consider the effect of varying the parameter n, with $g(0)$ fixed; these results are shown in figure 2–4. Let us first focus our attention on the zero-transpiration case (figure 2). We see that generally, over the range of values of n shown, two distinct solution branches exist. One of these is the well-known two-dimensional Falkner–Skan solution family (Rosenhead 1966), for which $W_0 \equiv 0$, which must be characterized by having $\theta_0(\eta) \equiv (1-n)U_{0\eta}(\eta)$, on account of (2.8) and (3.9). A second main solution family also exists, which is fully three dimensional in nature. For $n = 0$, the solutions here coincide precisely with the corner-flow solutions of DD and DSD. Additionally, in the particular case of $n = 1$, the two-dimensional solution is the classical Hiemenz solution (Rosenhead 1966), the other corresponds to the three-dimensional solution found by Davey & Schofield (1967) and Schofield & Davey (1967). The significance

† Note the typographical error in eqn (3.13) of DD, which should read $\Phi_{0\eta} \to 2 - \lambda$, $\Psi_0 \to \lambda$ as $\eta \to \infty$.

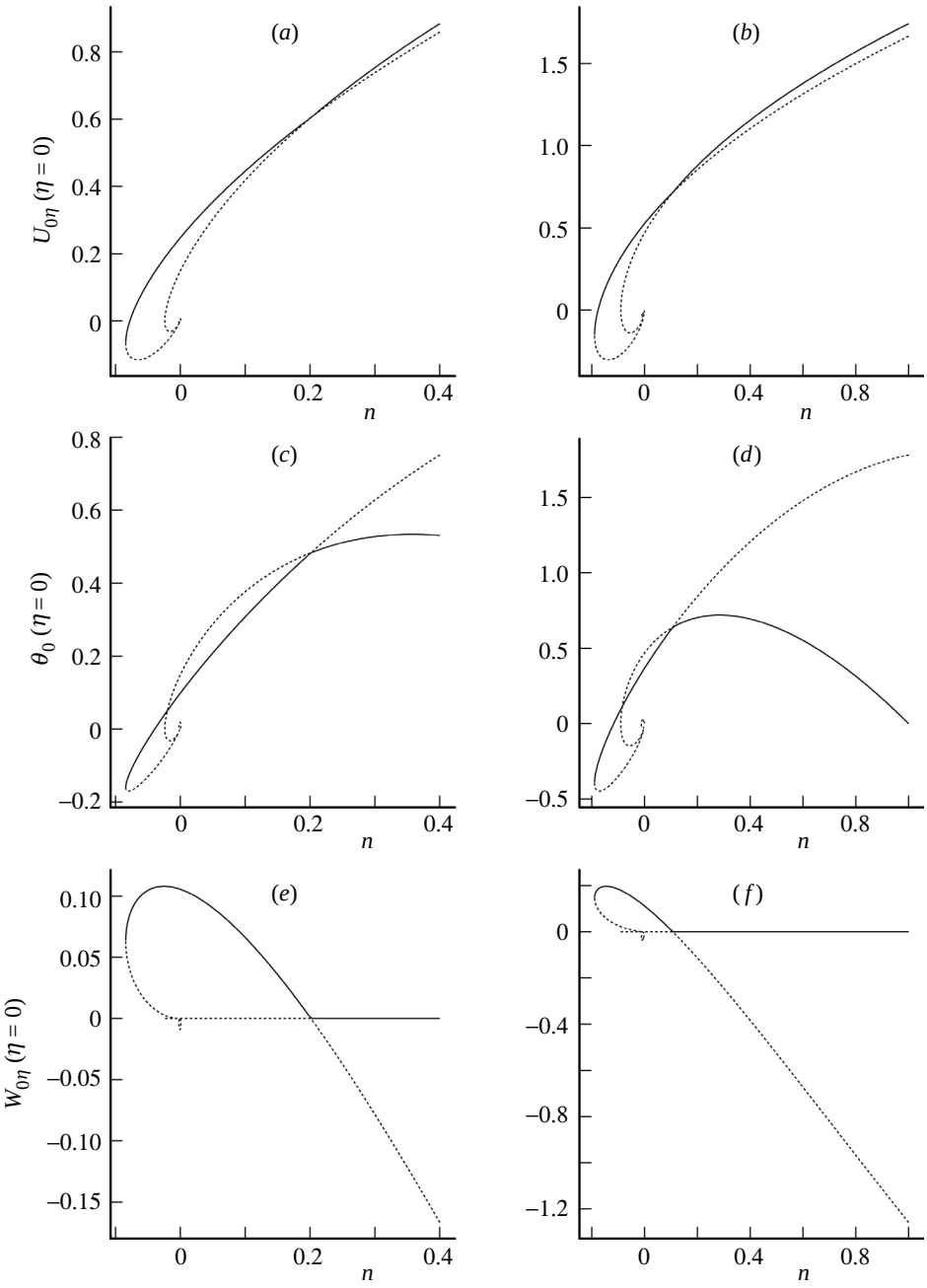

Figure 2. Solution curves: (*a*), (*c*) and (*e*) $g(0) = -0.5$; (*b*), (*d*) and (*f*) $g(0) = 0$.

of the solid and dashed lines will be explained later (in § 5). A selection of profiles for $U_0(\eta)$ and $W_0(\eta)$ for these main solution branches is shown in parts (*a*) and (*b*) of figure 5, respectively (noting that we must of course have $W_0(\eta) \equiv 0$ for the two-dimensional solution family). Non-uniqueness of the two-dimensional Falkner–Skan family of solutions is quite well known (Craven & Peletier 1972; Oskam &

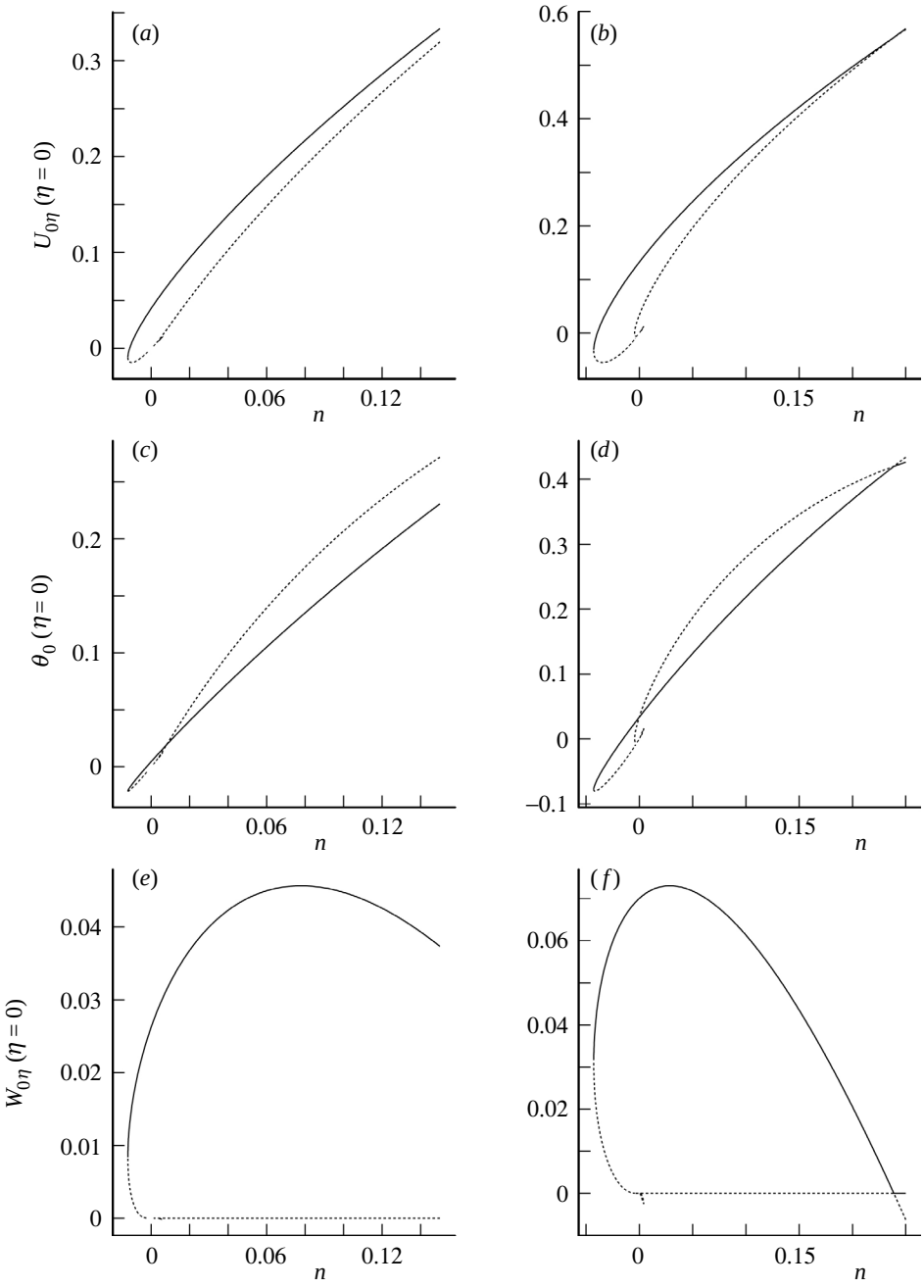

Figure 3. Solution curves: (*a*), (*c*) and (*e*) $g(0) = -1$; (*b*), (*d*) and (*f*) $n(g(0) = -0.75)$.

Veldman 1982), although these previous additional solution profiles are generally oscillatory in nature, at extreme values of n ($n < 0$ or $n > 1$), and are therefore unlikely to be realized in practice. The distributions of the velocity components as shown in figure 5 suggest entirely plausible velocity profiles for the additional

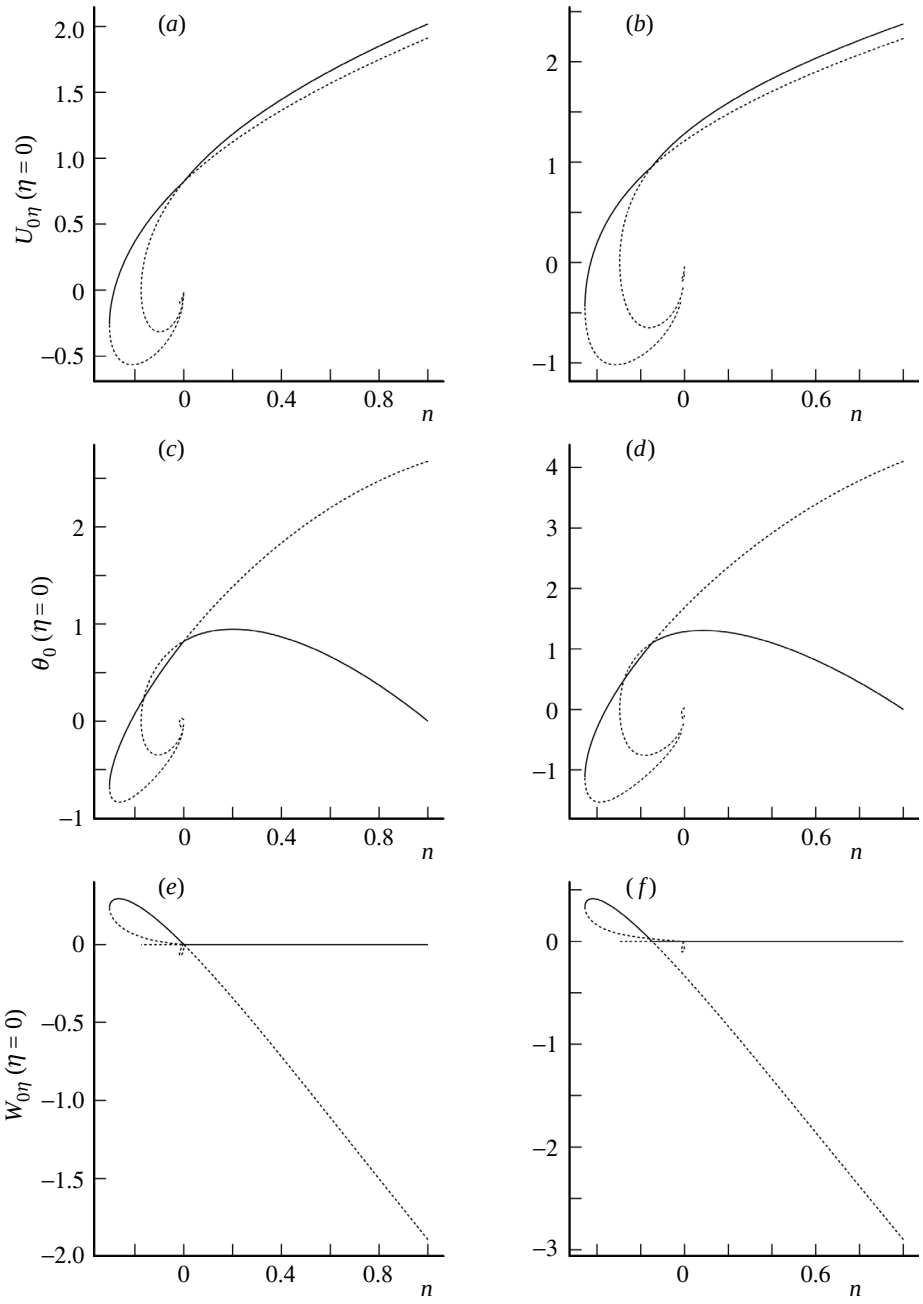

Figure 4. Solution curves: (*a*), (*c*) and (*e*) $g(0) = 0.456\,58$; (*b*), (*d*) and (*f*) $g(0) = 1$.

(three-dimensional) mode; note in particular the jet-like profile of the cross-flow. The distributions shown in these figures suggest that the reversed flow family of solutions involves a displaced shear layer; DSD suggested that in these regimes these layers become further displaced as $n \to 0$, i.e. as the origin is approached in the $g(0) = 0$ results in figure 2. In addition to the two main solution branches, there also exists a

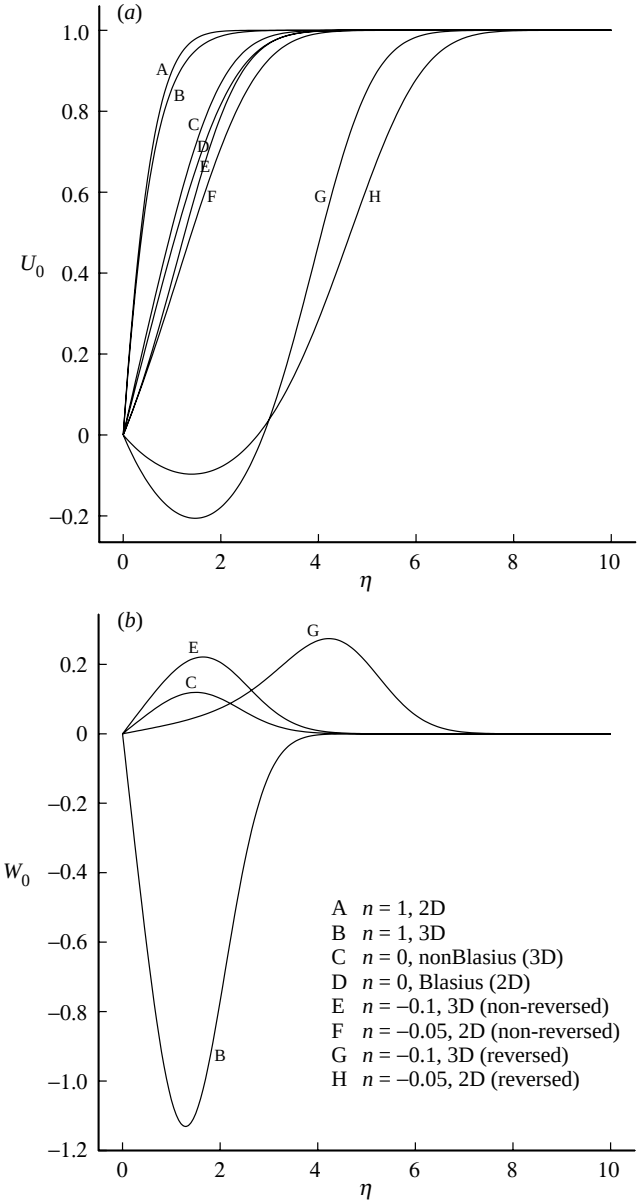

Figure 5. (*a*) Streamwise velocity profile ($\zeta \to \infty$) and (*b*) cross-flow velocity profiles ($\zeta \to \infty$). A, $n = 1$, two dimensional; B, $n = 1$, three dimensional; C, $n = 0$, non-Blasius (three dimensional); D, $n = 0$, Blasius (two dimensional); E, $n = -0.1$, three dimensional (non-reversed); F, $n = -0.05$, two dimensional (non-reversed); G, $n = -0.1$, three dimensional (reversed); H, $n = -0.05$, two dimensional (reversed).

small looped branch for $-0.0129\cdots < n < 0$, implying *six* solutions to the problem for $n = 0-$. Notice that one portion of this solution branch has $\theta_0(\eta = 0) < 0$, the other has $\theta_0(\eta = 0) > 0$, while both portions have $U_{0\eta}(\eta = 0) < 0$, corresponding to reversed flows. In the limit as $n \to 0-$, the four lower solution branches take on the

general form of a massively displaced shear layer, with a normal transpiration velocity on the lower edge of the shear layers, in the terminology of DSD corresponding to C_{2D}, C_{3Da} or C_{3Db}. The first of these is the well-known Chapman (1950) shear layer, the others being three-dimensional counterparts to this. In particular the shear layer associated with the two-dimensional solution is directly linked to C_{2D}, while for the small solution branch, the shear layer identified by having $\theta_0(\eta = 0) > 0$ together with the main three-dimensional solution branch are linked with the shear layer associated with C_{3Da}; the remaining small branch limiting solution (identified by exhibiting $\theta_0(\eta = 0) < 0$) is linked to C_{3Db}. Note too that the main solution branches cross (and are instantaneously identical) at $n = 0.167\ldots$ in this case. As the parameter $g(0)$ is decreased from zero (implying wall blowing; see figures 2 and 3), the small loop branch disappears, and also the two-dimensional and, subsequently, the three-dimensional solutions cease to exist for $n < 0$, the former occurring at $g(0) = -C_{2D}$, the latter occurring at $g(0) = C_{3Da}$. As $g(0)$ is increased above zero (corresponding to wall suction), we see from figure 4 that the crossing point of the two solution branches occurs at progressively smaller values of n, until at $n = 0.456\,58\ldots$ the coincidence point is at $n = 0$.

As $g(0)$ increases further, the two main solution branches remain separated, and the small loop solution also remains in existence. Note too that (in the light of the results of DD) other solution branches at more extreme values of n are also likely to exist.

It is straightforward to show that all these solutions are characterized by the condition

$$\theta_{0\eta}(0) = 2n^2 - 2n - \theta_0(0)g(0). \tag{3.11}$$

This is in contrast to the family of solutions (symmetrical about the line $\eta = \zeta$), considered by DSD, which were characterized by the condition

$$\theta_{0\eta}(0) = n^2 - \theta_0(0)g(0). \tag{3.12}$$

In the case of $n = 0$, it is confirmed that the problem considered here is identical to the corner-flow problem, as considered by DD and DSD. Finally, if there is no cross-flow at the outer edge of the boundary layer, as here, then the second-order terms in (3.1) are all zero.

4. Numerical scheme: full problem

We adopt a solution strategy similar to that used successfully in DD. Briefly, this used a second-order finite-difference scheme with standard successive relaxation methods, with the far-field ($\zeta \to \infty$) conditions being determined from the results of the previous section. Typically we took a grid size in the cross-flow direction of $\Delta\zeta = 0.1$ extending out to $\zeta = \zeta_\infty = 20$, and a grid in the normal direction of $\Delta\eta = 0.025$ extending out to $\eta = \eta_\infty = 20$.

We focus our attention on surface distortions of the form $H(\zeta) = \alpha e^{-\zeta^2}$ (where α is a constant), enabling symmetry to be invoked at $\zeta = 0$, and on zero freestream pressure gradient cases, i.e. $n = 0$, with no wall transpiration. For this choice of parameters, we note from figure 2 that there are two alternative far-field ($\zeta \to \infty$) conditions that may be imposed, namely Blasius flow or its three-dimensional 'cousin' (which we will refer to as the non-Blasius solution).

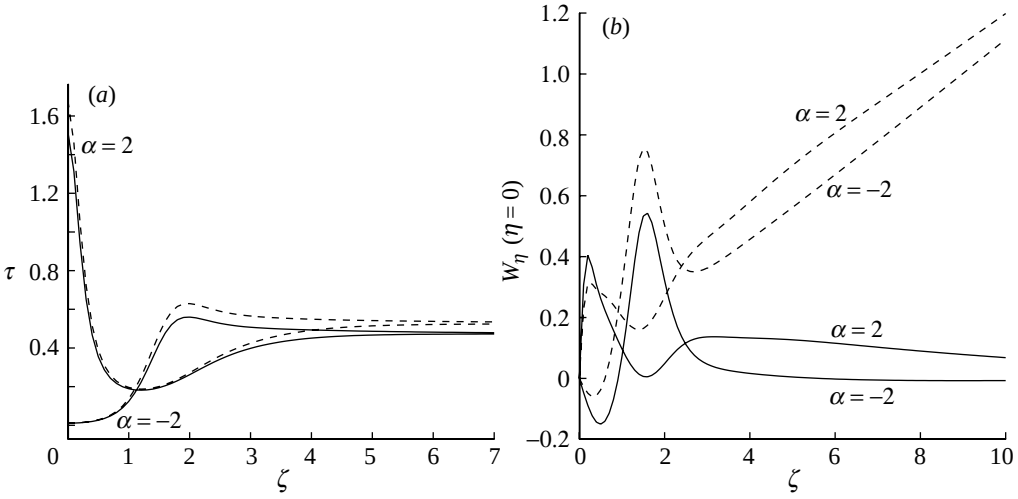

Figure 6. (*a*) Streamwise surface shear stress. (*b*) Cross-flow surface shear stress. (Solid lines denote Blasius far-field; dashed lines denote non-Blasius far-field.)

Figure 6*a*, *b* shows the distributions of streamwise and cross-flow components of wall shear stress corresponding to the two, alternative far-field flows, for $\alpha = \pm 2$; in these figures we have denoted flows corresponding to Blasius far-field conditions by solid lines, and non-Blasius far-field conditions by broken lines. Indeed, the differences between the Blasius and non-Blasius far-field flows are easily discernible in figure 6*b*, showing the cross-flow shear stress; in the latter case these distributions are clearly seen to grow linearly with ζ. The indentation ($\alpha = -2$) results show that close to the surface distortion there is a decrease in the streamwise shear stress (indicating the flow to be on the verge of separation); the converse is true for the $\alpha = 2$ results.

Parts (*a*) and (*b*) of figure 7 show the secondary velocity vectors for the Blasius and non-Blasius far-field conditions, respectively, for $\alpha = -2$; in both cases, the vertical scale is taken to be $\eta + H(\zeta)$, which is a better reflection of the true, physical, transverse coordinate than η. Both sets of results indicate a general drift of flow upwards (in spite of the indented nature of the surface, boundary-layer displacement effects must dominate here) and away from the distortion. The non-Blasius far-field case (figure 7*b*) exhibits the distinct, linearly increasing, jet-like profile as ζ increases, as alluded to earlier. In this case, fluid for this effect is clearly being entrained from the streamwise flow, which experiences a stronger retardation than in the case of Blasius flow in the far-field, as evidenced by comparison of the streamwise wall shear stresses between the two cases.

5. Discussion and further issues

In this paper we have focused our attention on self-similar solutions of the fully three-dimensional flow past a ridge. The non-uniqueness present in corner-flow boundary layers, discussed by DD and DSD, seems, in the light of the present study, not to be an isolated phenomenon, although the particular details are somewhat different; the suggestion here is that non-uniqueness in the context of boundary-layer flows is perhaps a much more common phenomenon than previously thought. Importantly,

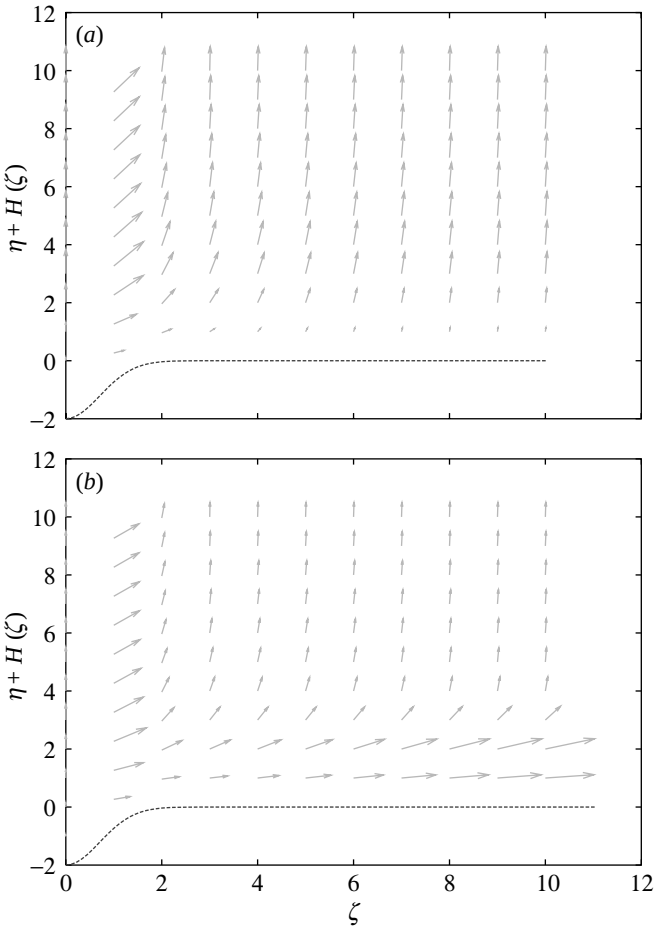

Figure 7. Secondary velocity vectors, $n = 0$ ((a) Blasius solution as $\zeta \to \infty$ and (b) non-Blasius solution as $\zeta \to \infty$), $\alpha = -2$.

the non-uniqueness revealed in the far-field study is wholly independent of any ridge profile, and hence is a totally generic phenomenon.

One question that arises is the nature of the spatial variation of the solution in non-similarity cases (i.e. when $F(x) \neq x^n$). In the corner-flow study of DSD it was found that standard, parabolic-type marching procedures were frequently ill posed, due to the existence of eigensolutions emanating from the leading edge. This turns out to be equally true here.

Specifically, let us consider the $|\zeta| \gg 1$ similarity solution described in § 3. We seek eigensolutions to the flow by writing the solution in the neighbourhood of $\xi = 0$ in the following form (as well as in Libby & Fox (1963), Chen & Libby (1968) and DSD, this type of approach is also suggested in the work on hypersonic boundary layers by Neiland (1970), Mikhailov *et al.* (1971) and Brown & Stewartson (1975)):

$$\left.\begin{aligned} U_0(\xi,\eta) &= U_{00}(\eta) + \xi^\lambda \tilde{u} + \cdots, & \Phi_0(\xi,\eta) &= \Phi_{00}(\eta) + \xi^\lambda \tilde{\phi} + \cdots, \\ \Psi_0(\xi,\eta) &= \Psi_{00}(\eta) + \xi^\lambda \tilde{\psi} + \cdots, & \theta_0(\xi,\eta) &= \theta_{00}(\eta) + \xi^\lambda \tilde{\theta} + \cdots. \end{aligned}\right\} \tag{5.1}$$

Substitution of these into the extended form of (3.2)–(3.5) (allowing for non-similarity effects; see eqns (2.36)–(2.39) of DSD) leads to the following system determining the perturbation quantities:

$$2\tilde{u} + (1-n)\lambda\tilde{u} = \tilde{\phi}_\eta + \tilde{\psi}, \tag{5.2}$$

$$\tilde{u}_{\eta\eta} = 4nU_{00}\tilde{u} + \lambda(1-n)U_{00}\tilde{u} - \tilde{\phi}U_{00\eta} - \tilde{u}_\eta\Phi_{00}, \tag{5.3}$$

$$\tilde{\theta} = \tilde{\psi}_\eta, \tag{5.4}$$

$$\tilde{\theta}_{\eta\eta} - (1-n^2)[U_{00}\tilde{u}_\eta + \tilde{u}U_{00\eta}] + \tilde{\theta}_\eta\Phi_{00} + \theta_{00\eta}\tilde{\phi} + \theta_{00\eta}\tilde{\phi} + \tilde{\psi}\theta_{00} + 2\tilde{u}\theta_{00} + \Psi_{00}\tilde{\theta} + 2U_{00}\tilde{\theta} + (n-1)\lambda\{-\theta_{00}\tilde{u} + U_{00}\tilde{\theta} + \tilde{\psi}U_{00\eta}\} = 0, \tag{5.5}$$

subject to the boundary conditions

$$\tilde{u}(0) = \tilde{\phi}(0) = \tilde{\psi}(0) = 0, \quad \tilde{u}, \tilde{\psi}, \tilde{\theta} \to 0 \quad \text{as } \eta \to \infty. \tag{5.6}$$

Here, the subscript 00 terms correspond precisely with the subscript 0 quantities considered in earlier sections of the paper. The system (5.2)–(5.6) was then tackled using two (independent) methods just as in DSD, namely

(i) a second-order finite-difference scheme, with the complete resulting homogeneous system being solved by a QZ algorithm; and

(ii) a local search routine, based on a fourth-order Runge–Kutta scheme.

Our *modus operandi* was to use (i) to provide initial estimates/starting values, and then (ii) to obtain refined estimates for the eigenvalue λ.

These computations generally yielded (just) real values of λ (i.e. λ_r). Figure 8 shows the variation of $(1-n)\lambda_r$ with n (it turns out that this quantity is rather more relevant to physical x-space than λ_r alone, on account of (2.10), and also remains bounded as $n \to 1$). In figure 8 we focus our attention solely on the main solution branches, for the zero transpiration case, $g(0) = 0$. For values of $n > 0.167\ldots$ (i.e. beyond the crossover point in figure 2), we find the two-dimensional branch only exhibits negative values of λ_r (in this regime, only the eigenvalue of smallest magnitude is shown), while for the three-dimensional branch there exists *one* real, positive eigenvalue (and many real, negative eigenvalues). The effect of this one eigenvalue is to indicate the existence of leading-edge eigensolutions, which render initial-value-type approaches to any spatially developing problem, based on these solutions, inappropriate. For $n < 0.167\ldots$, we see that there is a change-over: it is the two-dimensional solution branch that possesses the real and positive eigenvalue, while the three-dimensional solution branch only possesses eigenvalues with $\lambda_r < 0$ (again, only the eigenvalue of smallest magnitude is shown in this regime on figure 8). Note that although the $\lambda_r < 0$ eigenvalues have no relevance in the context of the leading-edge solution, nonetheless they are responsible in controlling the far-downstream development of solutions.

Intriguingly there is a further complexity which arises as soon as flow reversal occurs, namely where $U_{0\eta}(\eta = 0) < 0$; in these regimes we see many (probably an infinite number of) positive eigenvalues, for both two- and three-dimensional cases. This property seems entirely reasonable, given that the nature of the boundary-layer flow is likely to be elliptic in these regimes, and the multiplicity of leading-edge eigensolutions reflects this ellipticity.

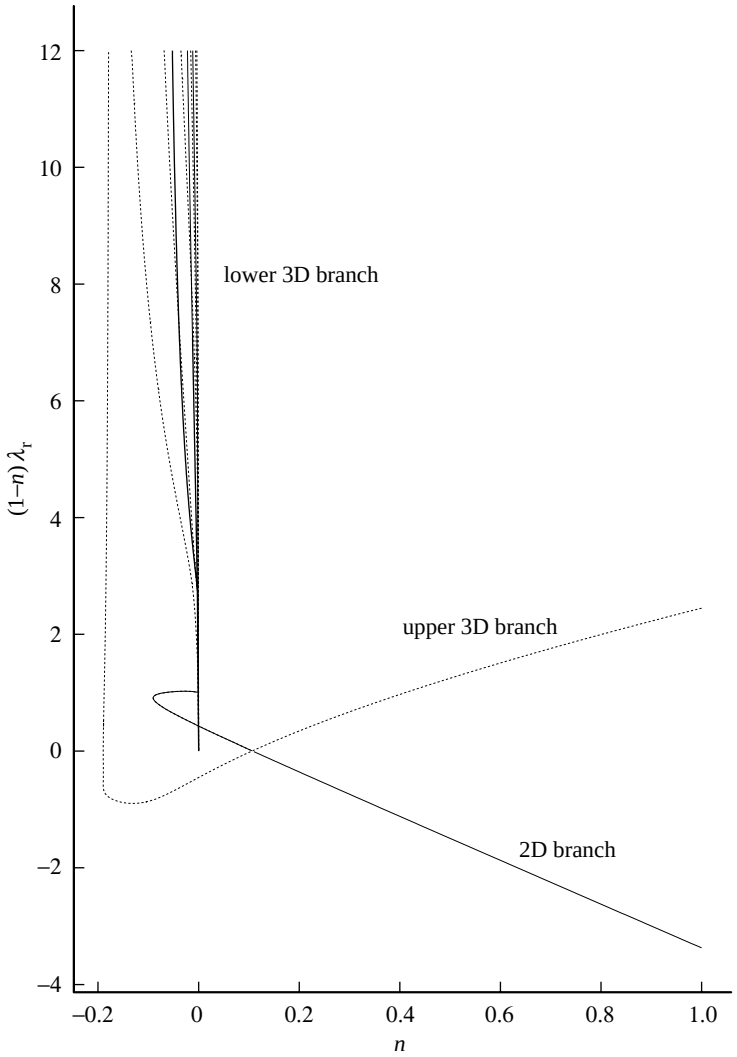

Figure 8. Spatial eigenvalues.

The significance of the solid and broken lines in figures 2–4 can now be revealed: namely that the solid lines refer to solutions *which do not possess any positive* λ_r, and hence solutions developing away from these similarity forms may be treated in the classical 'initial-value' fashion; the broken lines correspond to regimes *which possess at least one positive* λ_r.

From these, and all other computations performed to date, the following general trends emerge.

(1) For each value of n, at most only one solution does *not* possess a positive eigenvalue λ_r.

(2) It is the solution with the most positive value of $U_{0\eta}(\eta = 0)$ that possesses *only* negative values of λ_r.

(3) In cases of flow reversal, i.e. $U_{0\eta}(\eta = 0) < 0$, many (probably an infinite number of) positive λ_r exist.

The existence of these growing, leading-edge eigensolutions therefore has serious repercussions for treating the spatial development of solutions subject to three-dimensional disturbances (including, intriguingly for Blasius flow). However, the authors have successfully undertaken a number of computations involving spatially developing flows of this type, involving growing, leading-edge eigensolutions, using the quasi-elliptic approach described by DSD; these results are not shown here, but are qualitatively similar to the corner-flow results shown in DSD.

The authors gratefully acknowledge the support of NATO and the EPSRC.

References

Brown, S. N. & Stewartson, K. 1975 A non-uniqueness of the hypersonic boundary layer. *Q. J. Mech. Appl. Math.* **28**, 75.

Chapman, D. R. 1950 Laminar mixing of a compressible fluid. NACA Report 958.

Chen, K. K. & Libby, P. A. 1968 Boundary layers with small departures from the Falkner–Skan profile. *J. Fluid Mech.* **33**, 273.

Craven, A. H. & Peletier, L. A. 1972 On the uniqueness of solutions of the Falkner–Skan equation. *Mathematika* **19**, 135.

Davey, A. & Schofield, D. 1967 Three-dimensional flow near a two-dimensional stagnation point. *J. Fluid Mech.* **28**, 149.

Dhanak, M. R. & Duck, P. W. 1997 The effects of freestream pressure gradient on a corner boundary layer. *Proc. R. Soc. Lond.* A **453**, 1793.

Duck, P. W., Stow, S. R. & Dhanak, M. R. 1999 Non-similarity solutions to the corner boundary-layer equations (and the effects of wall transpiration). *J. Fluid Mech.* **400**, 125.

Hartree, D. R. 1937 On an equation occurring in Falkner and Skan's approximate treatment of the equations of the boundary layer. *Proc. Camb. Phil. Soc.* **33**, 223.

Libby, P. A. & Fox, H. 1963 Some perturbation solutions in laminar boundary-layer theory. *J. Fluid Mech.* **17**, 433.

Mikhailov, V. V., Neiland, V. Ya. & Sychev, V. V. 1971 The theory of viscous hypersonic flow. *A. Rev. Fluid Mech.* **3**, 371.

Neiland, V. Y. 1970 Upstream propagation of perturbations in a hypersonic flow with a boundary layer. *Akad. Nauk. SSSR Izv. Mekh. Zhid. i. Gaza.* **4**, 40.

Oskam, B. & Veldman, A. E. P. 1982 Branching of the Falkner–Skan solutions for $\lambda < 0$. *J. Engng Math.* **16**, 295.

Ridha, A. 1992 On the dual solutions associated with boundary-layer equations in a corner. *J. Engng Math.* **26**, 525.

Rosenhead, L. 1966 *Laminar boundary layers.* Oxford University Press.

Rubin, S. G. 1966 Incompressible flow along a corner. *J. Fluid Mech.* **26**, 97.

Schofield, D. & Davey, A. 1967 Dual solutions of the boundary-layer equations at a point of attachment. *J. Fluid Mech.* **30**, 809.

Stewartson, K. 1954 Further solutions of the Falkner–Skan equations. *Proc. Camb. Phil. Soc.* **50**, 454.